International Journal of Internet, Broadcasting and Communication Vol.16 No.1 169-175 (2024)
http://dx.doi.org/10.7236/IJIBC.2024.16.1.169

IJIBC 24-1-21

Enhancing Document Security with Computer Generated Hologram Encryption: Comprehensive Solution for Mobile Verification and Offline Decryption

Leehwan Hwang[1], Seunghyun Lee[2], Jongsung Choi[2],*

[1] *Assistant Professor, Department of Immersive Convergence Content, Kwangwoon University, Korea*
[2] *Associate Professor, Ingenium College, Kwangwoon University, Korea*
optics.hwang@kw.ac.kr, shlee@kw.ac.kr, jeschoi@kw.ac.kr:

Abstract

In this paper, we introduce a novel approach to enhance document security by integrating Computer Generated Hologram(CGH) encryption technology with a system for document encryption, printing, and subsequent verification using a smartphone application. The proposed system enables the encryption of documents using CGH technology and their printing on the edges of the document, simplifying document verification and validation through a smartphone application. Furthermore, the system leverages high-resolution smartphone cameras to perform online verification of the original document and supports offline document decryption, ensuring tamper detection even in environments without internet connectivity. This research contributes to the development of a comprehensive and versatile solution for document security and integrity, with applications in various domains.

Keywords: *Digital Hologram, Computer Generated Hologram, Convolutional neural network, artificial intelligence, Holography*

1. Introduction

In general, security codes used in today's society typically use barcodes or QR codes as markers for security. In general, security codes used in today's society typically use barcodes or QR codes as markers for security. These two markers not only have the information of the original document, but also serve as markers for security. However, recent advances in computer knowledge and technology have increased the possibility of counterfeiting or copying documents and code, and the number of counterfeiting and tampering cases such as ID cards, passports, and certificates of public institutions and product activation codes. For this reason, we propose to apply the type of the document to the holographic cryptographic decipherable security marker. Using CGH techniques with hologram algorithms, the document's type can be generated as a fringe pattern, printed and used as a security marker, and when the marker is decrypted, it can be reconstructed to the original document's type using the information from the reference wave from initial generation information.

Manuscript Received: December. 28, 2023 / Revised: January. 20, 2024 / Accepted: January. 29, 2024
Corresponding Author: jeschoi@kw.ac.kr
Tel:+82-2-940-5629
Associate Professor, Ingenium College, Kwangwoon University, Korea

2. Background Theory

2.1. CGH-based fringe pattern generation

In this research, we generated a CGH-based resilient encryption pattern and apply Pre-Training CNN to achieve the final performance improvement.

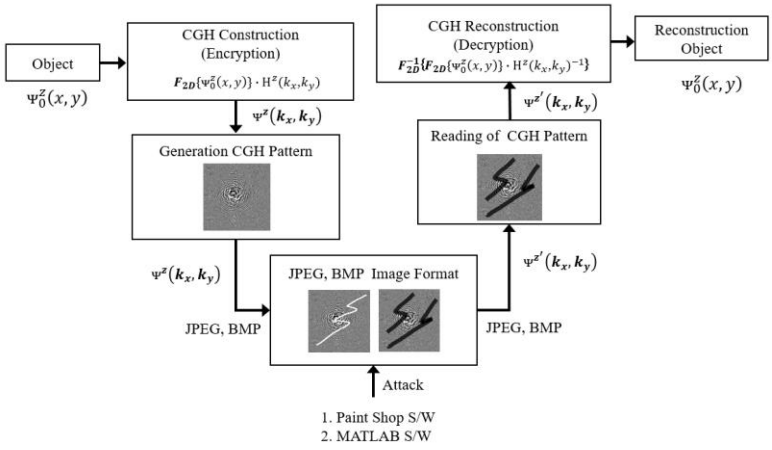

Figure 1. Flow for pattern generation and reconstruction process

Figure 1 is the process of using the optical scalar diffraction theory, which is the based on CGH to generate cryptographic patterns into JPEG and BMP format file with added various noise and losses and reconstruct them to compare the original and reconstructed results. Equation 2-1 is CGH-based pattern generation expression used in this study

$$\Psi^z(x,y) = \Psi_0^z(x,y) * h^z(x,y) = F_{2D}^{-1}[F_{2D}\{\Psi_0^z(x,y)\} \cdot H^z(k_x, k_y)] \quad (2\text{-}1)$$

In Equation 2-1, $\Psi^z(x,y)$ is a diffraction wave that progresses in the z-axis. $\Psi_0^z(x,y)$ is 2D image information such as documents and pictures for CGH pattern generation. For CGH-based processing, 2D information can be represented by converting it to a pixel matrix $\Psi_0^z(M,N)$). Here, M and N represent the entire pixel matrix (column M-row N) comprising 2D image information. $h^z(x,y)$ is the SFTF and k_x, k_y are the propagation constant in the x- and y-axis directions.

$$H^z(k_x,k_y) = \boldsymbol{F_{2D}}\{h^z(k_x,k_y)\} = e^{-j2\cdot\pi\cdot z\sqrt{\frac{1}{\lambda^2}-\left(\frac{p\cdot k_x}{k_0}\right)^2-\left(\frac{q\cdot k_y}{k_0}\right)^2}} \quad (2\text{-}2)$$

where p and q are $\frac{-M/2}{2} \le p \le \frac{+M}{2}-1, \frac{-N}{2} \le q \le \frac{+N}{2}-1$. M and N represent matrices of the same size created by converting 2D information into images, and are indexes representing the x and y axes, respectively.

λ(m) is the wavelength of the frequency used in the algorithm. In equation 2-2, $k_x = \frac{2\pi}{M\Delta x}$, $k_y = \frac{2\pi}{N\Delta y}$ and $k_0 = \frac{2\pi}{\lambda}$. In this expression, if we set the value of $\Delta x = \Delta y = i \cdot \lambda$ and select i as an integer $(i = 1,2,3..)$, we can have equation 2-3.

$$\mathrm{H}^z(k_x, k_y) = \mathrm{H}^z(\mathrm{p}, \mathrm{q}) = \mathrm{e}^{-\mathrm{j}2\cdot\pi\cdot\mathrm{z}\sqrt{\frac{1}{\lambda^2}-\left(\frac{p}{M\cdot i\cdot\lambda}\right)^2-\left(\frac{q}{N\cdot i\cdot\lambda}\right)^2}}$$

$$= \mathrm{e}^{-\mathrm{j}\cdot k_0\cdot\mathrm{z}\sqrt{1-\left(\frac{p}{M\cdot i}\right)^2-\left(\frac{q}{N\cdot i}\right)^2}} \quad (2\text{-}3)$$

As shown in Equation 2-3, we can see that $\Psi^z(x,y)$wave distance $+Z$, wavelength λ(mm), k_0 are a variable of $\mathrm{H}^z(k_x, k_y)$. Furthermore, p, q represents the pixel distance in the x- and y-axis directions. Equation 2-1 and 2-3 show that for each pixel of the CGH pattern, the corresponding values in the range $\frac{-M}{2} \le p \le \frac{+M}{2} - 1$ and $\frac{-N}{2} \le q \le \frac{+N}{2} - 1$ and both have information of $\mathrm{H}^z(k_x\,,\, k_y)$ values, respectively. Each pixel calculates an algorithm so that it can also have the value of the rest of pixels. And using this value to output to an image format of the same size as the 2D information allows us to extract the lost information from the values of the other pixels even if some of the pixels in the output image $\Psi^z(x,y)$are lost. The 2D information of $\Psi_0^z(x,y)$ from Equation 2-1 multiplied by $M(m,n)$ and the same size matrix $\mathrm{e}^{-\mathrm{j}\cdot 2\cdot\pi\cdot\mathrm{M(m,n)}}$ as $\Psi_0^z(x,y)$and the final value of $\Psi_0^z(x,y)$as shown in Equation 2-4.

$$\Psi^z(x,\mathrm{y}) = \boldsymbol{F}_{2D}^{-1}[\boldsymbol{F_{2D}}\{\Psi_0^z(x,y)\cdot\mathrm{e}^{-\mathrm{j}\cdot 2\cdot\pi\cdot\mathrm{M(m,n)}}\}\cdot\mathrm{H}^z(k_x,k_y)] \quad (2\text{-}4)$$

In this work, we use equation 2-4 to verify resilience. $\Psi_0^z(x,y)$ was multiplied by $\mathrm{e}^{-\mathrm{j}\cdot 2\cdot\pi\cdot\mathrm{M(m,n)}}$ and then made $\Psi_0^z(x,y)$ by binary (0,1). This binary pattern form allowed the output pattern to read the value $\Psi^{z'}(k_x,\, k_y)$ with the addition of damage as a paintshop or MALAB with minimal error.

2.2. Reconstruction of CGH image

Equations 2-5 show that $\Psi_0^z(x,y)$ requires $\mathrm{H}^z(k_x\,,\, k_y)$ information to enable reconstruction. Furthermore, since the spatial frequency transfer function of $\mathrm{H}^z(k_x, k_y)$ implies diffraction waves, it is possible to reconstruct circular information with some amount of information because the wave propagating from all pixels is a superimposed holographic property. To verify these properties, we restored the value $\Psi^{z'}(k_x,\, k_y)$ which forced the CGH pattern to be damaged by MALAB. Furthermore, we used Pre-Training CNN to maximize the resiliency of the reconstructed 2D original information by utilizing Equation 2-6. Learning time is needed to improve resilience by applying Deep Learning. To minimize this time, we leverage Pre-Training CNN to improve the reconstruction performance.

$$\Psi_0^z(x,y) = \boldsymbol{F}^{-1}\{\Psi^{z'}(k_x,\, k_y)\cdot\mathrm{H}^z(k_x,k_y)^{-1}\}\cdot\mathrm{e}^{\mathrm{j}\cdot 2\cdot\pi\cdot\mathrm{M(m,n)}} \quad (2\text{-}5)$$

3. Material and Method

For reconstruction various noise and losses by adding them to the output pattern image, we validated the information resiliency for the loss of $\Psi_0^z(x,y)$, a CGH-based 2D image. Furthermore, we compared and analyzed digital filters and Pre-Training CNN methods for noise rejection to improve the restore properties of restored images. The procedure for verification of reconstruction performance is shown in Figure 2. For analysis, equation 2-4 are utilized to generate cryptographic patterns of 2D images. The generated encryption pattern $\Psi^z(x,\mathrm{y})$ is output to JPEG and BMP files.

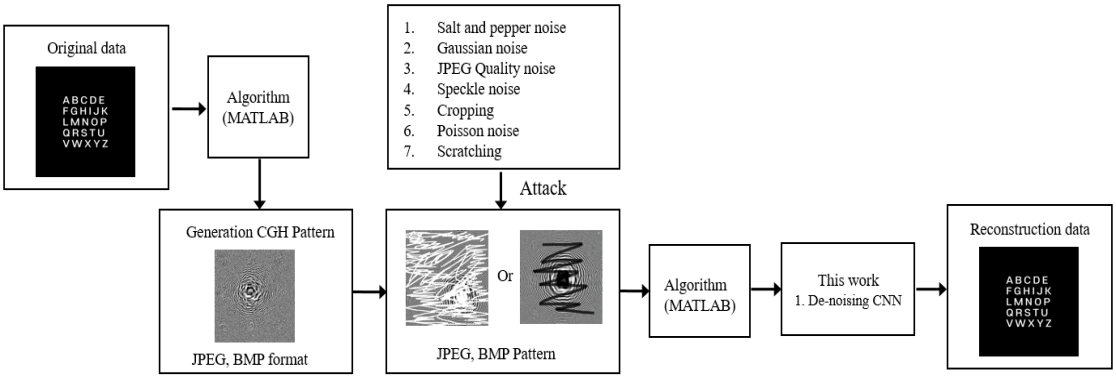

Figure 2. Verification process for reconstruction performance

The output file was loaded back into the Paint shop software or MATLAB adding noise or loss directly to the figure for causing problems with the encryption pattern. And then saving it back to the JPEP or BMP file to represent the value of $\Psi^{z'}(k_x,k_y)$. Equations 2-5 was used to reconstruct files having noise and loss information. Besides, to improve the information characteristics of the reconstructed 2D images according to the features of noise and loss, we verified the reconstruction performance by comparing various denoising filters with De-noise CNN techniques that have been recently studied. To compare the reconstruction performance, we compared the values of PSNR, CC, NCC, and Mean Square Error (MSE) of the final reconstructed image with 2D images based on noise and loss.

$$\mathrm{PSNR(dB)} = 10 \cdot log_{10}\left(\frac{255^2}{MSE}\right) \tag{2-6}$$

$$\mathbf{CC} = \frac{\sum_{i=1}^{M}\sum_{j=1}^{N}(I_{Original}(i,j) - I_{Original\_average}) \cdot (I_{Recovered}(i,j) - I_{Recoverd\_average})}{\sqrt{\sum_{i=1}^{M}\sum_{j=1}^{N}(I^2{}_{Original}(i,j) - I_{Original\_average})} \cdot \sqrt{\sum_{i=1}^{M}\sum_{j=1}^{N}(I^2{}_{Recovered}(i,j) - I_{Recoverd\_average})}} \tag{2-7}$$

where MSE is $\frac{1}{M\cdot \mathrm{N}}\sum_{i=1}^{M}\sum_{j=1}^{N}[I_{original}(i,j) - I_{attacked}(i,j)]^2$. Figure 3 is a pattern created using Equation 2-2. This pattern showed reconstruction results that did not artificially apply noise or loss.

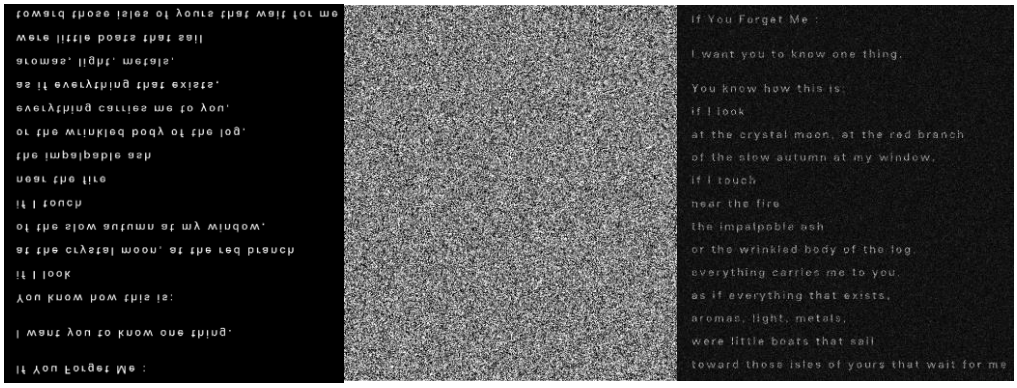

(a) **(b)** **(c)**

Figure 3. CGH conversion of the type of a document saved as a JPEG file: (a) 2D image file; (b) CGH pattern; (c) reconstruction result as a saved JPEG file format.

4. Results and Discussion

Figure 4 can presents a comparative analysis of eight different filtering techniques for mitigating Salt and Pepper noise, utilizing two performance metrics. Correlation Coefficient (CC) and the Peak Signal to Noise Ratio (PSNR). The left y-axis quantifies the CC, ranging from approximately 0.4 to 0.9, while the right y-axis measures the PSNR in decibels, extending from roughly 14 to 20 dB. The x-axis lists the filtering methods: 1) Adaptive Filter, 2) Gauss Filter, 3) Guided Filter, 4) Min.Filter, 5) MedianFilter, 6) Max.Filter, 7) Non filter, and 8) Deep Learning. The results indicate that the Adaptive Filter achieves the highest CC, whereas the Non filter records the lowest. In contrast, the Deep Learning approach registers the highest PSNR value, with the MedianFilter scoring the lowest. This visual representation allows for an immediate comparison of how each method performs in reducing Salt and Pepper noise, with blue lines and circles denoting CC and orange lines and squares indicating PSNR values.

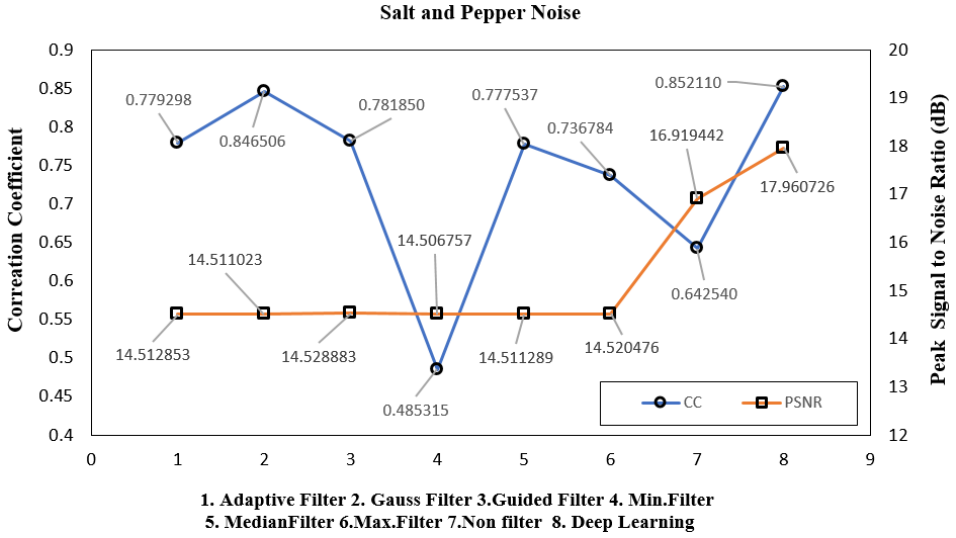

Figure 4. Characteristics of reconstruction with digital algorithm filters and Pre-training De-noise CNNs

4. Formatting your paper

Using numerical methods, we transformed the text of a document into a holographic interference pattern with CGH transformation algorithms based on interference of holographic wave and reference wave. In addition, amplitude-encoding was used to extract only the real part to decompose from a complex field containing amplitude and phase to an amount of pure amplitude. As a result, the CGH reconstruction algorithm with only the extracted real parts was used to verify the extent to which the original document was reconstructed by loading the amplitude value of the image. Unlikely conventional techniques, this study is differentiated from signal processing which uses pixel-stored data to reverse transformation. This work uses CGH as a data conversion technique that encodes into holographic interference patterns through CGH transformations of printed documents text in real-world and then reconstructs them through reference wave information, and verifies the encryption potential of documents through simulations.

5. Acknowledgement

This research was supported by the MSIT(Ministry of Science and ICT), Korea, under the ITRC(Information Technology Research Center) support program(IITP-2023-2020-0-01846) supervised by the IITP(Institute for Information & Communications Technology Planning & Evaluation)

6. Reference

[1] Thomas W.; Frey, H.; Jean Page. Virtual HUD using an HMD, Proceedings of SPIE - The International Society for Optical Engineering 2001, Volume 4361, Helmet- and Head-Mounted Displays VI.

[2] Choi, P.H.; Choi, Y.H.; Park, M.S.; Lee, S.H. Non-glasses Stereoscopic 3D Floating Hologram System using Polarization Technique, The Institute of Internet, Broadcasting and Communication 2019, Volume 8, Issue 1, pp. 18-23.

[3] Toshiaki, Y.; Nahomi M.; Kazuhisa Y. Holographic Pyramid Using Integral Photography, Proceedings of the 2nd World Congress on Electrical Engineering and Computer Systems and Science 2016, MHCI 109, pp. 16-17.

[4] Reichelt, S.; Haussler, R.; Fütterer, G.; Leister N. Depth cues in human visual perception and their realization in 3D displays, SPIE Proceedings, 2010, Volume 7690, pp. 111-112.

[5] De Silva, V.; Fernando, A.; Worrall, S.; Arachchi, H.K.; Kondoz, A. Sensitivity analysis of the human visual system for depth cues in stereoscopic 3-D displays. IEEE Transactions on Multimedia, 2011, Volume 13, No. 3, pp. 498-506.

[6] Krumholz, D.M.; Fox, R.S.; Ciuffreda, K.J. Short-term changes in tonic accommodation. Investigative Ophthalmology & Visual Science 1986, Volume 27, pp. 552-557.

[7] Avudainayagam, K. V.; Avudainayagam, C. S. Holographic multivergence target for subjective measurement of the astigmatic error of the human eye. Opt. Lett 2007, Volume 32, pp. 1926-1928.

[8] Ciuffreda, K.J.; Kruger, P. B. Dynamics of human voluntary acommodation, Am. J. Optom. Physiol 1988, Volume 65, pp. 365-370.

[9] Cacho, P., Garcia, A., Lara, F.; Segui, M. M. Binocular acommodative facilty testing reliabilty, Optom. Vis 1992, Volume 4, pp. 314-319.

[10] Bharadwaj S.R.; Candy T.R. Acommodative and vergence responses to conflicting blur and disparity stimuli during development, Journal of Vision 2009, Volume 9), pp. 1-18.

[11] Iribarren, R.; Fornaciari, A.; Hung, G. K. Effect of cumulative near work on accommodative facility and asthenopia, Int. Ophthalmol 2001, Volume 24, pp. 205-212.

[12] Rosenfield, M.; Ciufreda, K. J. Effect of surround propinquity on the open-loop accommodative response. Invest Ophthalmal 1991, Volume 32, pp. 142-147.

[13] Rosenfield, M.; Ciufreda, K. J.; Hung, G. K.; Gilmartin, B. Tonic accommodation: A review. I. Basic aspects. Ophthalmic Physiol 1993, Volume 13, pp. 266-284.

[14] McBrien, N.A.; Millodot, M. The relationship between tonic accommodation and refractive error. Investigative Ophthalmology & Visual Science 1987, Volume 28, pp. 997-1004.

[15] Krumholz, D.M.; Fox, R.S.; Ciuffreda, K.J. Short-term changes in tonic accommodation. Investigative Ophthalmology & Visual Science 1986, Volume 27, pp. 552-557.
[16] Nadezhda, V.; Pavel, S. Application of Photopolymer Materials in Holographic Technologies. polymers 2019, 11(12)
[17] Hanle, Z.; Huan, D.; Minyang, H.; Dahai, L.; Qionghua, Wang. Dual-View Integral Imaging 3D Display Based on Multiplexed Lens-Array Holographic Optical Element. Applied sciences 2019, 9(18).
[18] Maria, A. F.; Valerio, S.; Giuseppe, C. Volume Holographic Optical Elements as Solar Concentrators: An Overview. Applied sciences 2019, 9(18)
[19] Jung-ping, L.; Tatsuki, T.; Yoshio, H.; Ting-chung P. Incoherent Digital Holography: A Review. Applied sciences 2018, 8(1)
[20] Reid, V.; Adam, R.; Elvis C. S. C.; Terry, M. P. Hologram stability evaluation for Microsoft HoloLens. Spie 2017, Volume 10136.
[21] Oh, J. Y.; Park, J. H.; Park, J. M. Virtual Object Manipulation by Combining Touch and Head Interactions for Mobile Augmented Reality. Applied sciences 2019, 9(14).
[22] Takeda, T.; Hashimoto K.; Hiruma N.; Fukui Y. Characteristics of accommodation toward aparent depth. Vision Research 1999, Volume 39, pp. 2087-2097.
[23] Davies, L.N.; Mallen, E.A.; Wolffsohn, J.S.; Gilmartin, B. Clinical evaluation of the Shin-Nippon NVision-K5001/Grand Seiko WR-5100K autorefractor. Optom 2003, Volume 80, pp. 320-324.
[24] Gentet, P.; Gentet, Y.; Lee, S. H. Ultimate 04 the new reference for ultra-realistic color holography. In Emerging Trends Innovation in ICT(ICEI), 2017 International Conference on IEEE, 2017, pp. 162-166.
[25] Gentet, P.; Gentet, Y.; Lee, S. H. New LED's wavelengths improve drastically the quality of illumination of pulsed digital holograms. In Digital Holography and Three-Dimensional Imaging, 2017, pp. 209.
[26] Moses, L. E. Non-parametric statistics for psychological research. Psychological Bulletin, 1952, Volume 49, No. 2, pp.122-143.
[27] Andrew, J. K. Parametric versus non-parametric statistics in the analysis of randomized trials with non-normally distributed data. BMC Medical Research Methodology, 2005, Volume 5, No. 35.
[28] Davison, M. L.; Sharma, A. R. Parametric statistics and levels of measurement. Psychological Bulletin, 1988, Volume 104, pp.137-144.